Theor. Comput. Fluid Dyn. (2005) 00: 1–15
DOI 10.1007/s00162-005-0164-6

ORIGINAL ARTICLE

Q. X. Wang · K. S. Yeo · B. C. Khoo · K. Y. Lam

Vortex ring modelling of toroidal bubbles

Received: 5 January 2004 / Accepted: 17 February 2005 / Published online: 10 May 2005
© Springer-Verlag 2005

Abstract During the collapse of a bubble near a surface, a high-speed liquid jet often forms and subsequently impacts upon the opposite bubble surface. The jet impact transforms the originally singly-connected bubble to a toroidal bubble, and generates circulation in the flow around it. A toroidal bubble simulation is presented by introducing a vortex ring seeded inside the bubble torus to account for the circulation. The velocity potential is then decomposed into the potential of the vortex ring and a remnant potential. Because the remnant potential is continuous and satisfies the Laplace equation, it can be modelled by the boundary-integral method, and this circumvents an explicit domain cut and associated numerical treatment. The method is applied to study the collapse of gas bubbles in the vicinity of a rigid wall. Good agreement is found with the results of Best (J. Fluid Mech. **251** 79–107, 1993), obtained by a domain cut method. Examination of the pressure impulse on the wall during jet impact indicates that the high-speed liquid jet has a significant potential for causing damage to a surface. There appears to be an optimal initial distance where the liquid jet is most damaging.

Keywords Toroidal bubbles · Boundary-integral method · Potential flow theory

1 Introduction

During the collapse of a bubble in the neighborhood of a rigid boundary, the greater mobility of the fluid away from the boundary causes the surface of the bubble to collapse faster than elsewhere, thereby causing the formation of a liquid jet on the far side of the bubble. The liquid jet threads the bubble and ultimately impacts upon the opposite face of the bubble nearest to the rigid boundary. This jetting phenomenon was first observed experimentally by Benjamin and Ellis [1]. The transition of a bubble surface from singly-connected to doubly-connected induces circulation in the flow around the toroidal bubble.

A significant part of the potential energy in the initial high-pressure bubble is transformed into the kinetic energy of the high-speed liquid jet. The moment of the jet is primarily concentrated in one direction, and clearly has a potential for causing damage to the surface upon which it strikes. This is the main mechanism of damage to hydraulic machinery by cavitation bubbles, as well as damage to vessels by underwater explosion bubbles. It has long been an important research field ever since the beginning of last century. To date, the most successful numerical modelling of bubble dynamics has been based on the boundary integral spatial solution

Communicated by J. R. Blake

Q. X. Wang (✉)
Maritime Research Centre, Division of Environmental and Water Resources Engineering, School of Environmental and Civil Engineering, Nanyang Technological University, 50 Nanyang Avenue, Singapore 630798, The Republic of Singapore
E-mail: cqxwang@ntu.edu.sg

K. S. Yeo · B. C. Khoo · K. Y. Lam
Department of Mechanical Engineering, National University of Singapore, 10 Kent Ridge Crescent, Singapore 19260, The Republic of Singapore

coupled with time integration, i.e. the mixed-Eulerian-Lagrangian method (MEL). Axisymmetric MEL was implemented for the motion of a bubble near a rigid wall by Guerri et al. [2], Blake et al. [3], Baker and Moore [4], Best and Kucera [5], Brujan et al. [6], and others. It was also employed to simulate the interaction of a bubble with a nearby free surface by Blake and Gibson [7], Blake et al. [8, 9], and Wang et al. [10, 11].

Three-dimensional MEL was implemented for the motion of a bubble near an inclined wall or a solid structure by Chahine [12], Chahine et al. [13], Wilkerson [14], Harris [15, 16], Blake et al. [9], Wang [17, 18], Pozrikidis [19], and Wang and Khoo [20]. General reviews on bubble dynamics may be found in Plesset and Prosperetti [21], Blake and Gibson [22], and Blake et al. [9].

The evolution of a toroidal bubble poses an interesting theoretical problem of practical importance. Nevertheless, there has been only a few works on the dynamics of toroidal bubbles. The solution of the Laplace equation in a doubly-connected domain is non-unique. Best [23] introduced a domain-cut, rendering the domain singly-connected. Across the domain-cut, the potential function is discontinuous, and the potential jump equals the circulation of the flow along any closed path passing through the eye of the torus. The cut, deforming with the evolution of the bubble, requires special numerical treatment. Best [24], Pearson et al. [25, 26] improved this domain-cut approach by fixing the domain cut. Zhang et al. [27] and Zhang and Duncan [28] presented a hypersingular boundary-integral method for toroidal bubbles. Their method models the continuous jet impact and the formation of a vortex sheet around the jet surface. Szymczak et al. [29] assumed inviscid incompressible flow and used a finite-difference method. They simulated a bubble collapse near a rigid wall including jet impact, but their model needs more CPU time and memory since it is based on a field approach.

Benjamin and Ellis [1] postulated that, upon jet impact, the bubble must transform into a vortex-ring bubble to conserve the Kelvin impulse of the flow. Pedley [30] made a theoretical study for a vortex-ring bubble assuming its cross-section is circular. Lundgren and Mansour [31] simulated the evolution of a bubble ring at constant volume, with a vortex ring seeded inside, using a dipole distribution on the bubble surface. In this paper, the concept of Lundgren and Mansour is applied to model a toroidal bubble formed during bubble collapse. A vortex ring is introduced inside the bubble torus just after jet impact to account for the circulation in the flow. The potential is then decomposed into the potential of the vortex ring and a remnant continuous potential, which is modelled by the boundary-integral method. The vortex-ring model obliviates the need for any explicit domain cut.

To investigate the mechanism of damage of a collapsing bubble, it is important to study the pressure impulse acting on the wall during jet impact. The development of the liquid jet, the jet impact, and the evolution of a toroidal bubble cause numerical instabilities, which prohibits the calculation of $\frac{\partial \phi}{\partial t}$ needed for the pressure evaluation. Preliminary calculations of the pressure impulse on the wall are performed and analyzed in this work for a bubble initially positioned at various distances from the wall.

The time-integration boundary-integral method for a singly-connected bubble is briefly described in Sect. 2. The vortex-ring modelling of a toroidal bubble is presented in Sect. 3. Section 4 describes the numerical results on the evolution of toroidal bubbles as well as the pressure history on the rigid boundary. Section 5 summarizes the present work.

2 Boundary-integral method

We consider the evolution of a gas bubble near a horizontal infinite rigid wall, as shown in Fig. 1. The fluid in the time-varying domain Ω, bounded by the bubble surface and the wall, is assumed to be inviscid and incompressible, and the flow is assumed to be irrorational. A cylindrical polar coordinate system (r, θ, z) is adopted with its z-axis along the axis of revolution, pointing against the direction of gravity, the rigid wall is located at $z = 0$. The velocity potential $\phi(\mathbf{p})$ satisfies the boundary-integral equation

$$c(\mathbf{p})\phi(\mathbf{p}) = \int_{\partial\Omega} \left(\frac{\partial \phi(\mathbf{q})}{\partial n} G(\mathbf{p}, \mathbf{q}) - \phi(\mathbf{q}) \frac{\partial G(\mathbf{p}, \mathbf{q})}{\partial n} \right) \mathrm{d}S(\mathbf{q}), \tag{1}$$

where $\mathbf{p}$ is the field point and $\mathbf{q}$ the source point. The $c(\mathbf{p})$ is the solid angle subtended by the bubble surface at point $\mathbf{p}$ on the fluid side; $c(\mathbf{p}) = 2\pi$ for point $\mathbf{p}$ on a smooth surface and 4π for an interior fluid point. $\partial\Omega$ is the bubble surface; $\mathbf{n}$ is the unit outward normal vector of the fluid domain Ω on $\partial\Omega$; $G(\mathbf{p}, \mathbf{q}) = |\mathbf{p} - \mathbf{q}|^{-1} + |\mathbf{p} - \mathbf{q}'|^{-1}$ is the half-space Green function, with $\mathbf{q}'$ being the reflected image of $\mathbf{q}$ across the wall. The no-penetration condition on the rigid boundary, $\frac{\partial \phi}{\partial n} = 0$, and the boundary condition at infinity, $|\nabla \phi| \to 0$, are satisfied automatically by (1).

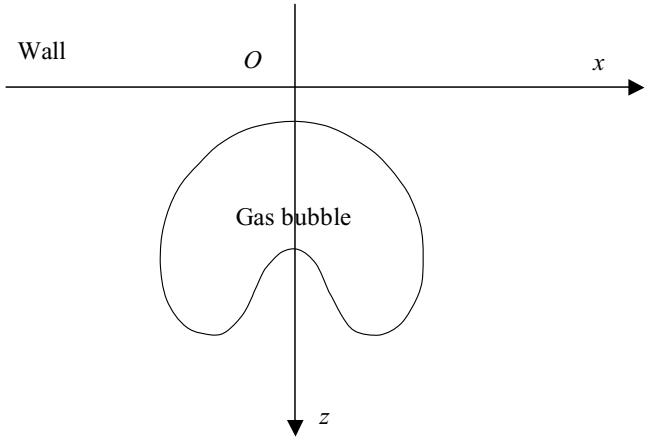

Fig. 1 The evolution of a gas bubble near a horizontal wall

The pressure inside the gas bubble p_b, consists of the vapor pressure p_c, and the pressure of the non-condensing gas, which is assumed to follow the adiabatic law,

$$p_\mathrm{b} = p_\mathrm{c} + p_0 \left(\frac{V_0}{V}\right)^\lambda, \tag{2}$$

where V_0 and p_0 are the initial volume and pressure of the non-condensable gas of the bubble, and λ is the ratio of the specific heats of the gas; in this work, we take $\lambda = 1.25$ corresponding to the adiabatic constant for explosive TNT gaseous products.

The evolution of the bubble is subjected to the kinematic and dynamic boundary conditions, requiring that a point on the bubble surface remains on the surface, and the pressure is continuous across the bubble surface,

$$\frac{\mathrm{d}\mathbf{x}}{\mathrm{d}t} = \nabla\phi. \tag{3}$$

$$\frac{\mathrm{d}\phi}{\mathrm{d}t} = \frac{p_\infty}{\rho} + \frac{1}{2}|\nabla\phi|^2 - g\,(z - z_0) - \frac{1}{\rho}\left(p_\mathrm{c} + p_0\left(\frac{V_0}{V}\right)^\lambda\right), \tag{4}$$

where g is the gravitational acceleration, and $\mathrm{d}/\mathrm{d}t$ the material derivative following particles on the bubble surface. The centre of the spherical bubble at the initial instant lies in the plane $z = z_0$, and p_∞ is the ambient pressure on this plane. The surface tension has been neglected in (4), as it is only important for tiny bubbles, with radii less than a millimeter [9].

We non-dimensionalize the variables with respect to the pressure $\Delta p = p_\infty - p_\mathrm{c}$ and the maximum radius R_m of the bubble, where R_m denotes the maximum radius that the bubble would attain if it is allowed to evolve in an infinite fluid domain under the same pressure condition. The normalized dynamical boundary condition (4) becomes

$$\frac{\mathrm{d}\phi}{\mathrm{d}t} = 1 + \frac{1}{2}|\nabla\phi|^2 - \delta^2\,(z - \gamma) - \varepsilon\left(\frac{V_0}{V}\right)^\lambda, \tag{5}$$

where $\delta = \sqrt{\rho g R_\mathrm{m}/\Delta p}$ is the buoyancy parameter, $\varepsilon = p_0/\Delta p$ the normalized initial bubble pressure, and $\gamma = z_0/R_\mathrm{m}$ the normalized initial distance of the bubble centre from the wall.

The numerical modelling is briefly described as follows, more details can be found in Blake et al. [3] and Wang et al. [10, 11]. Because the bubble surface is axisymmetric, it can be described by its intersect with the plane $\theta = 0$. The intersect is then discretized as N linear elements, each of which is locally parameterized by ξ in the range [0,1]. N is chosen as $N = 100$ in this work. Following Taib [32], the integrals in Eq. (1) can be integrated over the discretized bubble surface to yield

$$c(r_0, z_0)\phi(r_0, z_0, t) = \sum_{j=1}^{N}\int_0^1 \left(\psi(\xi)K_1(r, z, r_0, z_0, t) - \phi(\xi)K_2(r, z, r_0, z_0, t)\right)\mathrm{d}\xi, \tag{6}$$

where the potential $\phi(\xi)$ and its normal derivative $\psi\ (\xi) = \frac{\partial \phi}{\partial n}$ are approximated with linear functions defined by their values at the end nodes of each element. The kernel functions K_1 and K_2 are given by

$$K_1(r, z, r_0, z_0, t) = \frac{4rK(k)}{D}\sqrt{\left(\frac{\mathrm{d}z}{\mathrm{d}\xi}\right)^2 + \left(\frac{\mathrm{d}r}{\mathrm{d}\xi}\right)^2}, \tag{7a}$$

$$K_2(r, z, r_0, z_0, t) = -\frac{4rK(k)}{D^3}\left\{\frac{2r_0}{k^2}\frac{\mathrm{d}z}{\mathrm{d}\xi}K(k) + \left[\frac{\mathrm{d}z}{\mathrm{d}\xi}(r + r_0) - \frac{\mathrm{d}z}{\mathrm{d}\xi}(z - z_0) - \frac{2r_0}{k^2}\frac{\mathrm{d}z}{\mathrm{d}\xi}\right]\frac{E(k)}{1 - k^2}\right\}, \tag{7b}$$

where $D = \sqrt{(r + r_0)^2 + (z - z_0)^2}$ and $k = \frac{2}{D}\sqrt{r_0 r}$; $K(k)$ and $E(k)$ are the complete elliptic integrals of the first and second kind [33].

The bubble is assumed to begin evolving at $t = 0$ as a high-pressure spherical bubble of radius R_0 with zero radial velocity. The quiescent initial state is prescribed, i.e., $\phi = 0$ throughout the entire fluid domain. The initial radius R_0 is solved by reverse time integration of the Rayleigh equation from the normalized maximum radius of 1.0 to R_0 [5],

$$R\ddot{R} + \frac{3}{2}\dot{R}^2 = \varepsilon\left(\frac{R_0}{R}\right)^{3\lambda} - 1. \tag{8}$$

Multiplying Eq. (8) one can be reformulated after multiplication by $2R^2\dot{R}$ to yield

$$\frac{\mathrm{d}}{\mathrm{d}t}\left(R^3\dot{R}^2\right) = 2\varepsilon R_o^{3\lambda} R^{2-3\lambda} - 2R^2\dot{R}.$$

The equation can then be integrated analytically, subject to $\dot{R} = 0$ at $R = R_0$ and $R = 1$, to give the following relationship between the initial bubble radius R_0 and the strength parameter ε:

$$2\varepsilon\frac{R_o^{3\lambda} - R_0}{1 - 3\lambda} = \frac{2}{3}\left(1 - R_0^3\right). \tag{9}$$

At each time step, the normal velocity component on the bubble and free surfaces is calculated with the boundary integral method, and the normal vector and tangential velocity vector are calculated with the surface interpolation. With the material velocity calculated, the bubble surface and the velocity potential on it are then updated by integrating (3) and (5) using the predictor-corrector scheme. With the known right-hand side of (5), a variable time step can be chosen to ensure the maximum change in the velocity potential is a small prescribed value, chosen as 0.03.

3 Toroidal bubble model

Consider the jet impacting on the opposite bubble surface wall, as shown in Fig. 2a. Suppose the impact of the jet on the bubble surface occurs at a single point (an idealized case), and the bubble shape and velocity potential distribution on it are not affected by the initial contact of the surfaces (cf. [23]). The breaking up and merging of the liquid surfaces during jet impact were discussed recently by Keller et al. [35]. In the axisymmetric case, the impact point lies on the symmetry axis at nodes 1 and $N + 1$, as shown in Fig. 2a. The fluid domain is doubly-connected after jet impact, and the flow solution is non-unique. To solve the problem, a vortex ring is introduced inside the toroidal bubble. The strength of the vortex-ring is the circulation Γ of the flow along a closed path that threads through the torus, which is equal to the jump of the potential ϕ across the contact points at the impact time,

$$\Gamma = \oint_C \nabla\phi \cdot \mathrm{d}\mathbf{l} = \phi_{N+1} - \phi_1, \tag{10}$$

where ϕ_1 and ϕ_{N+1} are potentials at the impact point. For an incompressible potential flow, the circulation Γ is invariable in time [23]. Zhang et al. [27] simulated and discussed the difference of the potentials at the two poles versus time before jet impact. They noticed that the difference increases with time before impact.

Next, we decompose the velocity potential ϕ into two parts: the potential φ_{vr} of the vortex-ring of strength Γ, and a single-valued remnant potential φ

$$\phi(r, z, t) = \varphi^{\mathrm{vr}}(r, z) + \varphi(r, z, t). \tag{11}$$

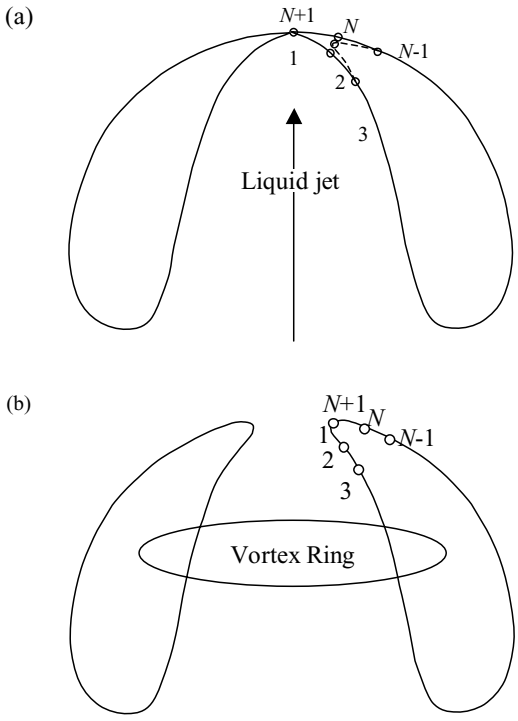

Fig. 2 Numerical transition of bubble shape **a** immediately before and **b** immediately after jet impact

For an axisymmetric case, the vortex ring is a circle with centre at the symmetry axis. In theory, the precise placement or location of the vortex ring (or loop) is immaterial so long as it lies completely within the toroidal bubble. To avoid possible numerical instability, the vortex-ring should not be too close to the bubble surface. In this paper, the initial location of the vortex ring is chosen to be at the mean position of the bubble surface nodes, i.e. the radius a of the vortex ring and height of its centre $z = c$ along the symmetry axis are obtained as follows:

$$a = \frac{1}{N+1}\sum_{j=1}^{N+1} r_j, \quad c = \frac{1}{N+1}\sum_{j=1}^{N+1} z_j. \tag{12}$$

In the course of simulation, the vortex ring is relocated when it is too close to the evolving bubble surface.

When the toroidal bubble is created, the remnant potential φ on the bubble surface that is needed for further simulation is calculated from (11). For this purpose, one needs to first calculate the velocity potential φ^{vr} on the bubble surface due to the vortex ring. The computation, which is based on the Biot-Savart law, is described in detail below. We note that the velocity potential φ^{vr} of the vortex ring is discontinuous. However, the total velocity potential $\phi(r, z, t) = \varphi^{\mathrm{vr}}(r, z) + \varphi(r, z, t)$ is a continuous function of space. The same computation of the remnant potential φ on the bubble surface is also carried out whenever the vortex ring is repositioned due to the changing geometry of the bubble.

The numerical transform of a singly-connected bubble to a toroidal one is carried out by removing nodes 1 and $N + 1$ corresponding to the impact point, repositioning their immediate nodes 2 and n at their mean position, and redefining the bubble surface along the dashed line (Fig. 2a). Remnant potential φ at nodes 2 and N are replaced by their mean value. The bubble surface and the remnant potential on it are then re-interpolated into its doubly-connected shape and re-discretized, as shown in Fig. 2b. The removed part of the boundary is of the element size, but has been greatly exaggerated in Fig. 2b for clarity.

The velocity field of a circular vortex ring of radius of a, strength Γ, centered at the origin can be calculated from the Biot-Savart law

$$\mathbf{v}_0^{\mathrm{vr}}(r, z) = \frac{\Gamma}{4\pi}\oint_C \frac{\mathbf{dl} \times (\mathbf{p} - \mathbf{q})}{|\mathbf{p} - \mathbf{q}|^3} = \frac{\Gamma}{4\pi}\frac{a}{d^3}\left\{ f(k)\mathbf{e}_r + \left(2\pi a F\left(\tfrac{5}{4}, \tfrac{7}{4}, 2; k^2\right) - x f(k)\right)\mathbf{e}_z \right\}. \tag{13}$$

where $\mathbf{e}_r$ and $\mathbf{e}_z$ are unit vectors of the cylindrical polar coordinates, $d = \sqrt{r^2 + z^2 + a^2}$, $k = 2ar/d^2$, and $f(k) = \frac{4}{k} - \frac{2}{k\sqrt{1-k}} - \frac{2}{k\sqrt{1+k}} + \frac{3}{4}\pi k F(\frac{3}{4}, \frac{5}{4}, 1; k^2)$. $F(a, b, c, x)$ is the hyper-geometrical function (Abramowitz and Stegun, 1965 [33]).

The velocity field of a circular vortex ring of radius a, and strength Γ, centered at $z = c$ along the z-axis near a wall at $z = 0$ is found by the image method to be

$$\mathbf{v}^{\mathrm{vr}}(r, z) = \mathbf{v}_0^{\mathrm{vr}}(r, z - c) + \mathbf{v}_0^{\mathrm{vr}}(r, z + c). \tag{14}$$

The potential $\varphi^{\mathrm{vr}}(r, z)$ necessarily vanishes at infinity. Its value at a point $s_j = (r_j, z_j)$ on the bubble surface may be obtained by integrating the velocity field

$$\varphi^{\mathrm{vr}}(r_j, z_j) = \varphi^{\mathrm{vr}}(r_1, z_1) + \int_{s_1}^{s_j} \mathbf{v}^{\mathrm{vr}}(r, z) \cdot \mathrm{d}\mathbf{l}. \tag{15}$$

Here $\varphi_{\mathrm{vr}}(r_1, z_1)$ is the potential of the vortex ring at node 1 of the bubble surface

$$\varphi^{\mathrm{vr}}(r_1, z_1) = \int_{-\infty}^{z_1} w^{\mathrm{vr}}(0, z)\, \mathrm{d}z + \int_{0}^{r_1} u^{\mathrm{vr}}(r, z_1)\, \mathrm{d}r, \tag{16}$$

where $u^{\mathrm{vr}}(r, z)$and $w^{\mathrm{vr}}(r, z)$ are r- and z-components of $\mathbf{v}^{\mathrm{vr}}(r, z)$.

The potential of the vortex ring satisfies the Laplace equation in the fluid domain and decays at infinity. The remnant potential φ thus satisfies the Laplace equation in the flow domain and also decays at infinity too, and therefore satisfies (6). Substituting (11) into (3) and (5) yields the kinematic and dynamic boundary conditions for the remnant potential φ on the bubble surface,

$$\frac{\mathrm{d}\mathbf{x}}{\mathrm{d}t} = \nabla\varphi + \mathbf{v}^{\mathrm{vr}}, \tag{17}$$

$$\frac{\mathrm{d}\varphi}{\mathrm{d}t} = 1 - \mathbf{v}^{\mathrm{vr}}(\nabla\varphi + \mathbf{v}^{\mathrm{vr}}) + \frac{1}{2}|\nabla\varphi + \mathbf{v}^{\mathrm{vr}}|^2 - \delta^2(z - \gamma) - \varepsilon\left(\frac{V_0}{V}\right)^{\gamma}. \tag{18}$$

Both of the original potential ϕ and remnant potential φ satisfy the Laplace equation, and thus satisfy the boundary integral equations (1) and (6). The boundary conditions (17)–(18) for the remnant potential φ are in the same form as those for the original potential ϕ in Eqs. (3) and (5). Therefore, the remnant potential φ can be solved using the boundary-integral method and updated in time in the same manner as that for original potential ϕ of the pre-toroidal bubble, as described in Sect. 2.

4 Numerical analysis

4.1 Collapse of pre-toroidal bubbles

We first briefly describe the bubble behavior before jet impact, which will be useful in analyzing the evolution of a toroidal bubble and the pressure impulse on the wall. The bubble considered here is characterized by the strength parameter $\varepsilon = 100$, and is initiated at various distances γ from the rigid wall. We set buoyancy parameter $\delta = 0$, for consistency with the results of Best [23] with which a comparison will be made.

Figure 3 shows the collapse of the bubble initially located at $\gamma = 1.5, 1.0, 0.75$, and 0.5 from the wall. The wall is located at $z = 0$ in this figure as well as in all other figures in this section. For $\gamma = 1.5$ (Fig. 3a), the bubble remains roughly spherical during most of the collapse phase, except that it takes a kidney shape and a liquid jet forms in a very short period at the end of the collapse phase. For $\gamma = 1.0$ (Fig. 3b), the liquid jet forms slightly earlier in the collapse phase as compared to the previous case, and the jet is larger and sharper in form. As the bubble is placed closer to the rigid wall at $\gamma = 0.75$ (Fig. 3c) and $\gamma = 0.50$ (Fig. 3d), the near face of the bubble is squashed against the wall during the later stage of the expansion phase. The liquid jet forms earlier and hits the wall once it penetrates the bubble.

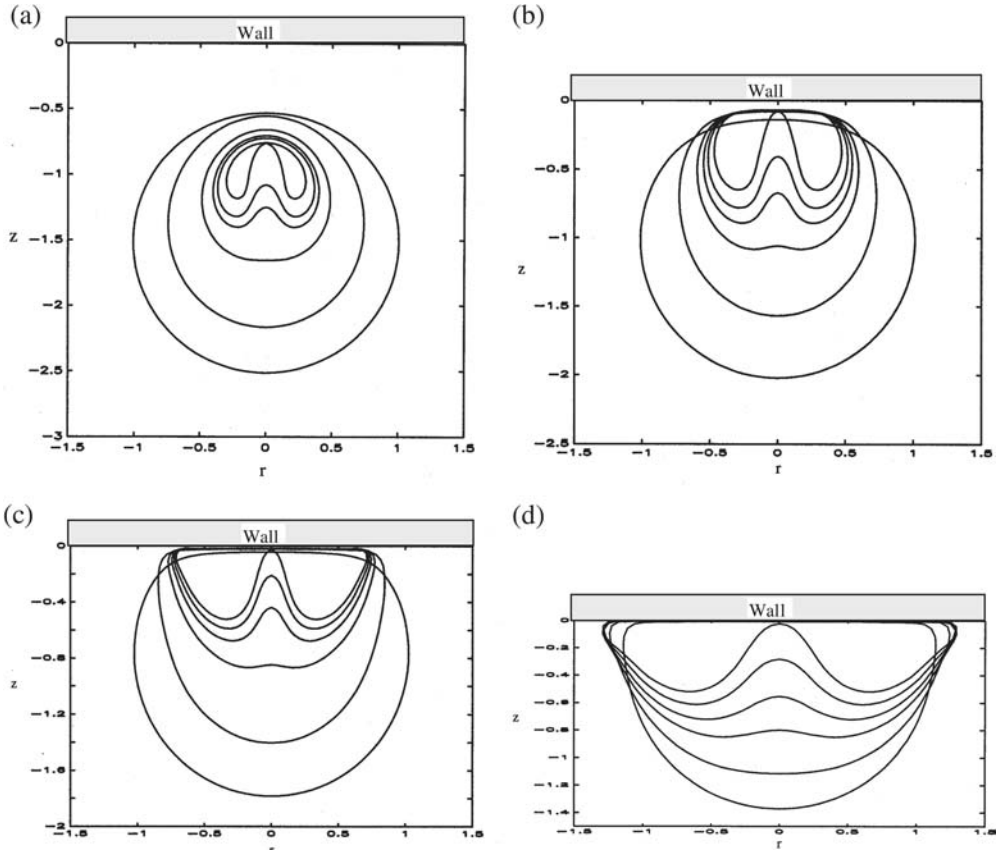

Fig. 3 Bubble evolution during collapse for $\varepsilon = 100$, $\delta = 0.0$: **a** $\gamma = 1.5$ at $t = 1.093$ (outermost), 1.842, 2.077, 2.129, 2.148, 2.182 (innermost), **b** $\gamma = 1.0$ at $t = 1.153$ (outermost), 1.887, 2.110, 2.170, 2.202, 2.229 (innermost), **c** $\gamma = 0.75$ at $t = 1.124$ (outermost), 1.929, 2.104, 2.156, 2.189, 2.232 (innermost), and **d** $\gamma = 0.5$ at $t = 1.148$ (outermost), 1.458, 1.758, 1.866, 1.965 (innermost)

The Kelvin impulse of a bubble was introduced by Benjamin and Ellis [1], and was further developed by Blake et al. [3, 8, 9] into a criterion for determining the directions of the re-entrant jet and the migration of the bubbles. The Kelvin impulse is defined as

$$\mathbf{I} = \int_{\partial\Omega_b} \phi \mathbf{n} \, \mathrm{d}S, \tag{19}$$

where $\partial\Omega_b$ denotes the bubble surface.

The jet tip velocity and Kelvin impulse versus time are given in Fig. 4a and b, respectively. The jet tip accelerates sharply towards the end of the collapse phase. Comparing the four cases, we observe that, as the bubble is initiated closer to the wall, the remnant volume at jet impact increases; the jet tip velocity at the end of the collapse phase (just prior to the impact) decreases, and the Kelvin impulse of the bubble increases.

4.2 Evolution of toroidal bubbles

The first case of toroidal bubbles to be considered is for a bubble with $\varepsilon = 100$ and $\delta = 0$ initiated at $\gamma = 2.0$. At jet impact, the *circulation* Γ around a closed path threading the torus is -4.30. From Fig. 5a, one can observe that the bubble continues to collapse (or shows a reduction in volume) for a very short time after jet penetration. In this short period of time, the cross-sectional area of the impact region increases rapidly to the diameter of the liquid jet, whilst the rest of the bubble surface continues to shrink more slowly. Upon reaching its minimum volume, the bubble begins to rebound (re-expand in volume). The rebounding

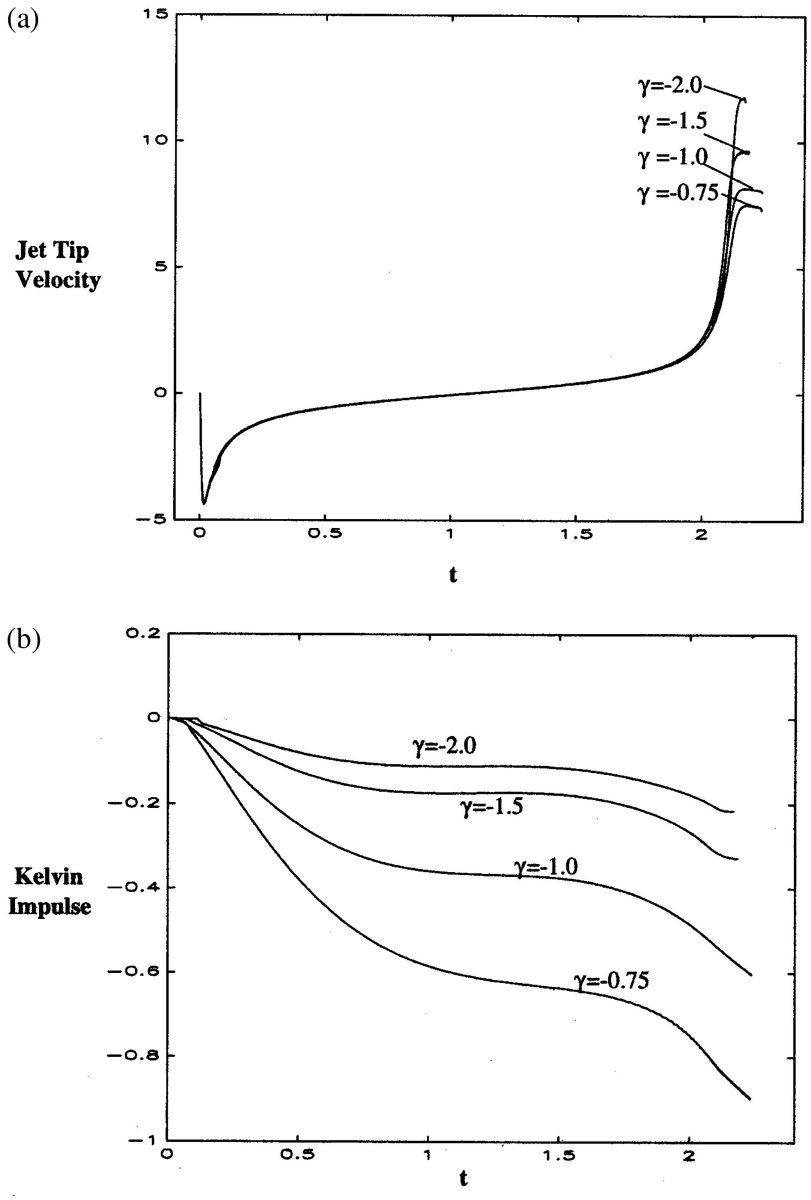

Fig. 4 **a** The jet tip velocity before jet impact and **b** Kelvin impulse versus time for the bubble with $\varepsilon = 100$ and $\delta = 0.0$ initiated at distances $\gamma = 2.0$, 1.5, 1.0 and 0.75 from a rigid wall

sequences of the bubble in toroidal form are shown in Fig. 5b. There is a small protrusion on the surface of the bubble corresponding to the position of jet impact. This protrusion actually deepens slightly during the initial rebound, but disappears rapidly as the rebounding progresses. It is well known that a bubble is drawn towards a rigid surface during collapse due to the Bjerknes effect [3]. In terms of centroid motion, it can be seen that the bubble in Fig. 5b is also attracted towards the wall during its rebounding. This is a further computational affirmation of the presence of a Bjerknes-type effect, the original Bjerknes effect was introduced by Bjerknes (cf. [[34], Ch. 11]) to explain the attraction of spheres, pulsating at small amplitude, to a rigid surface. In our case, however, not only is the distortion of the bubble surface is large, but the bubble has undergone a true topological transition from a sphere to a torus.

The next case concerns the bubble initiated at $\gamma = 1.5$. This case has been investigated in great detail by Best [23]. The jet impact occurs at time $t = 2.183$ with a *circulation* strength of $\Gamma = -4.72$, as acquired by the flow around the toroidal bubble. The corresponding results obtained by Best are $t = 2.189$ and $\Gamma = -4.63$. Figure 6 compares the present results (dashed line) at (a) $t = 2.182$ (immediately after jet impact),

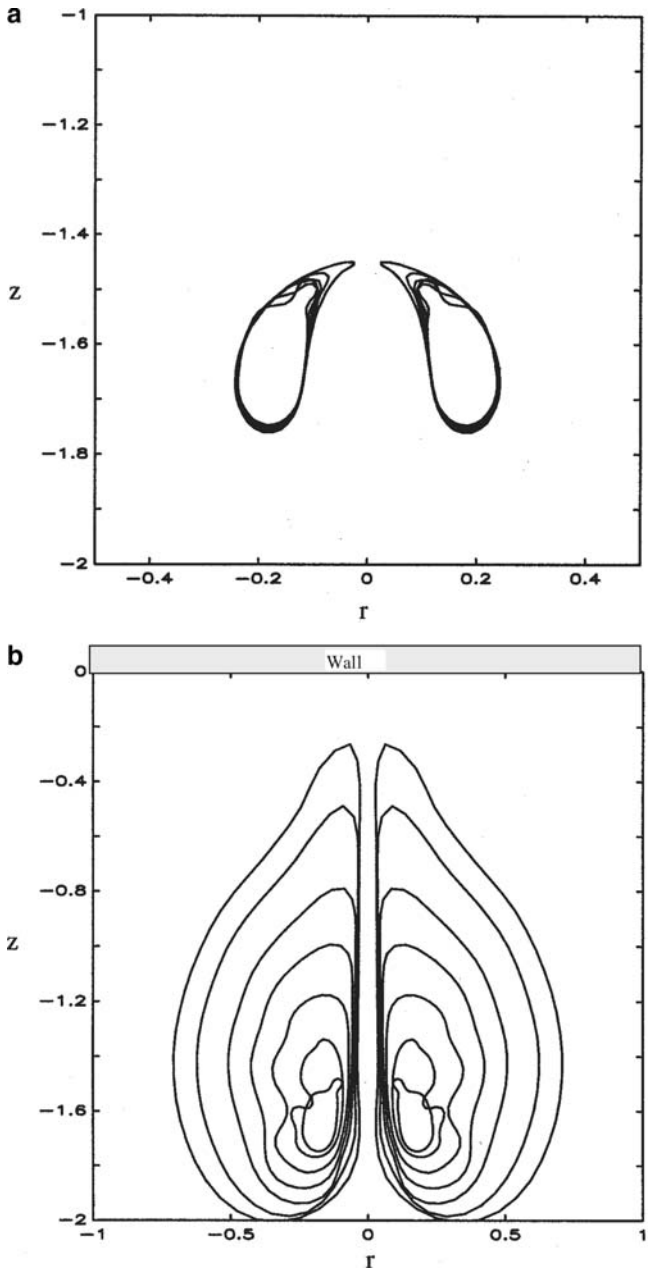

Fig. 5 Evolution of the toroidal bubble follows the collapse of a bubble with $\varepsilon = 100$, $\delta = 0.0$, and $\gamma = 2.0$. The circulation is $\Gamma = -4.300$. During **a** the collapse at $t = 2.165$ (outermost), 2.167, 2.168, 2.170, 2.173 (innermost), and **b** the rebounding phase at $t = 2.173$ (innermost), 2.193, 2.222, 2.259, 2.306, 2.392, 2.475 (outermost)

(b) $t = 2.385$, and Best's results (solid line) at (a) $t = 2.189$ (immediately after jet impact (b) $t = 2.386$, respectively. The bubble profiles in the two approaches agree well immediately after jet impact (Fig. 6a), except that a smaller cut is made in the present procedure to construct the post-impact toroidal bubble. This may be due to a larger cut is needed in the branch cut approach, in order to handle the intersecting and matching the cut with the bubble surface. On the whole the bubble profiles of the two approaches agree at the other corresponding time step (Fig. 6b). These are small differences in the timings and bubble profiles, which might be due to the numerical implementation of the topological transition and surgical cut of bubble boundary. Without experimental data available for comparison, it is difficult to judge which model is more accurate. Best's results also depict the evolution of the domain-cut, and his model breaks down as the cut line pushes against the rigid wall (see Fig. 6b). The vortex ring approach that we have presented does not suffer

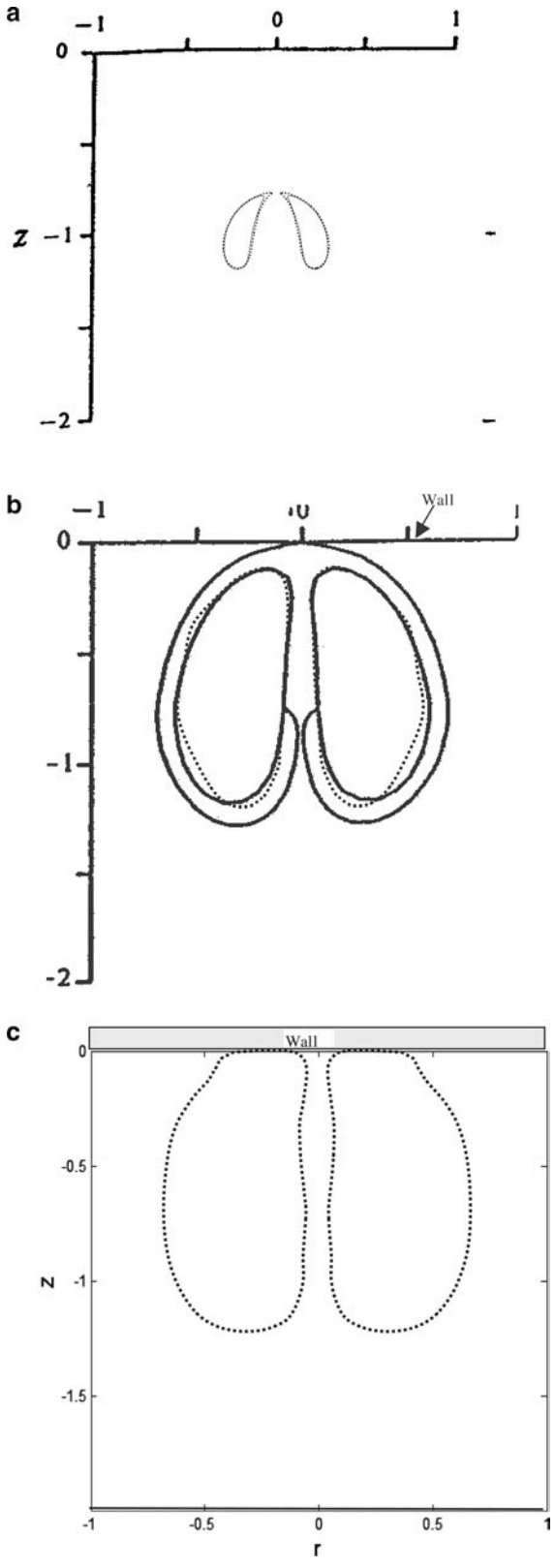

Fig. 6 Evolution of the toroidal bubble follows the collapse of a bubble with $\varepsilon = 100$, $\delta = 0.0$, and $\gamma = 1.5$. The present results (dashed line) at **a** $t = 2.182$ (immediately after jet impact), **b** $t = 2.385$, and **c** $t = 2.496$. The results of Best (1993) (solid line) at **a** $t = 2.189$ (immediately after jet impact), **b** $t = 2.386$

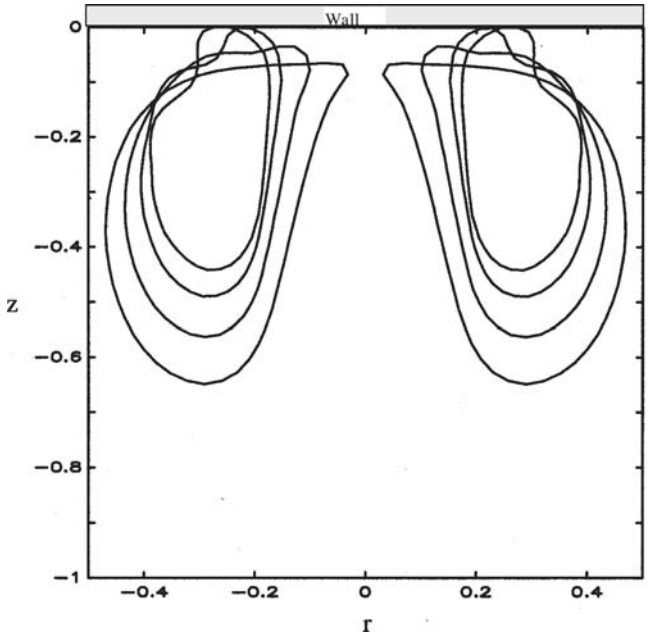

Fig. 7 Evolution of the toroidal bubble that evolves from the collapse of a bubble with $\varepsilon = 100$, $\delta = 0.0$, and $\gamma = 1.0$. The circulation is $\Gamma = -4.992$. During the collapse at $t = 2.229$ (outmost), 2.235, 2.244, 2.245 (innermost)

from the cut-line limitation. Our simulation lasted until the bubble rebounded right into the rigid boundary (Fig. 6c).

The last case is for a bubble initiated even closer to the rigid wall at $\gamma = 1.0$ (Fig. 7). In this case, the top surface of the bubble is already partially flattened against the wall as the liquid jet comes into contact with it and bursts forth upon the wall. The bubble surfaces near the wall are pushed outwards by the impacting jet, creating an increasing area of impact on the wall and a broader jet. Meanwhile, the toroidal bubble continues to collapse to a smaller volume. The bubble surface practically touches the rigid wall in the process, before there is any opportunity for the bubble to rebound.

4.3 Pressure impulse on a rigid wall

To investigate the possibility of a collapsing bubble causing damage to a surface, we consider the distribution and history of fluid pressure acting on the surface during bubble collapse. The evolution of the pressure $p_{\mathrm{bc}}(t)$ at the centre point of the rigid boundary with time is shown in Fig. 8 for the case of a bubble initiated at $\gamma = 2.0$ with $\varepsilon = 100$ and $\delta = 0$. The first maximum at time $t = 0$ is derived from the initiation of the bubble. At this time, the pressure inside the bubble is very large. This pressure, and indeed all subsequent pressure changes, are instantaneously communicated to the wall by the incompressible liquid medium. $p_{\mathrm{bc}}(t)$ decreases very rapidly during the early part of the expansion phase of the bubble along with the decrease of gas pressure inside the bubble. Then the pressure assumes a small value, fairly close to hydrostatic pressure of the far field p_∞, throughout most of the expansion and collapse phases. Near the end of the collapse phase, the pressure increases very sharply to a second peak around the time of the impact of the liquid jet onto the opposite bubble surface. The second pressure peak of $p_{\mathrm{bc}} = 22.4$, arising from the impact of the jet, is 34% higher than the first peak of $p_{\mathrm{bc}} = 16.7$ produced during bubble initiation. The distribution of pressure $p_{\mathrm{b}}(r)$ over the rigid wall is shown in Fig. 9 at three instances, corresponding to the inception of the bubble, just prior to jet impact and just after jet impact. As expected, the wall pressure decreases in the radial direction. The pressure at the centre point on the rigid boundary is increased by over 70% upon jet impact, and the post-impact pressure distribution also displays a sharper radial gradient near the centre.

Three more sets of centre pressure histories $p_{\mathrm{bc}}(t)$ are presented in Fig. 10 for the bubble initiated at the distances of $\gamma = 1.5$, 1.3, and 1.2, respectively. These time histories are similar to that for $\gamma = 2.0$ given in Fig. 8; a high pressure at bubble inception, near hydrostatic pressure level over much of the expansion and collapse phases, and a very sharp second pressure peak generated during the time of jet impact. Comparing

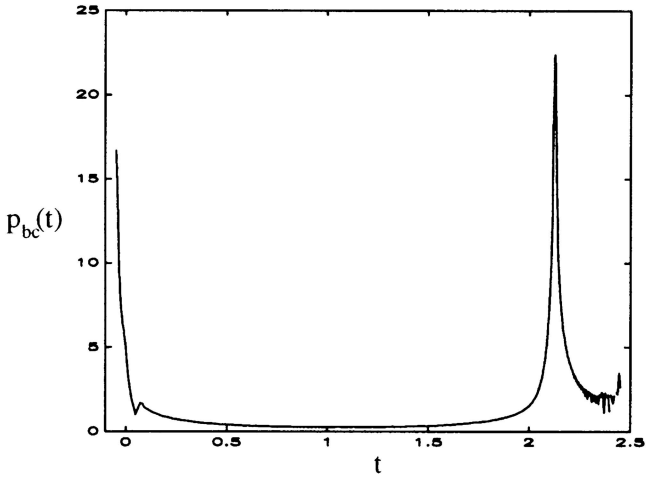

Fig. 8 The variation of pressure $p_{bc}(t)$ at the center point of the rigid boundary with time for a bubble with $\varepsilon = 100$ and $\delta = 0.0$ initiated at $\gamma = 2.0$ from the rigid wall

the four cases, one can see that the initial pressure on the wall at $t = 0$ is increased as the bubble is initiated closer to the rigid wall. This is not surprising. The more interesting feature is the variation of the second pressure peak with the initiation distance of the bubble γ from the wall. The second pressure peak at first increases in magnitude as γ is reduced from 2.0 to reach a maximum p_{bc} value of about 38.2 around γ of 1.3. At $\gamma = 1.3$ (Fig. 10b), the jet-induced peak pressure is about 53% higher than the pressure produced at bubble inception. At $\gamma = 1.2$, the jet-induced pressure peak drops back significantly to a value of 28.3. This shows that there is an optimal initiation distance for which a collapsing bubble may be most damaging to the wall.

The mechanism underlying the above phenomenon can be explained as follows. As the bubble is initiated closer to the wall, the bubble jet is closer to the wall. But, the bubble volume at jet impact increases (Figs. 3a–3d), and so does the remnant energy of the bubble, therefore, less bubble energy has been transformed into the jet moment. As a result, the jet tip velocity as well as the jet momentum at the end of the collapse phase (just prior to the impact) decreases with γ. It is possible that there is an optimal initial distance for which a collapsing bubble may be most damaging to the wall. Further experimental and numerical investigations are needed to confirm this behaviour.

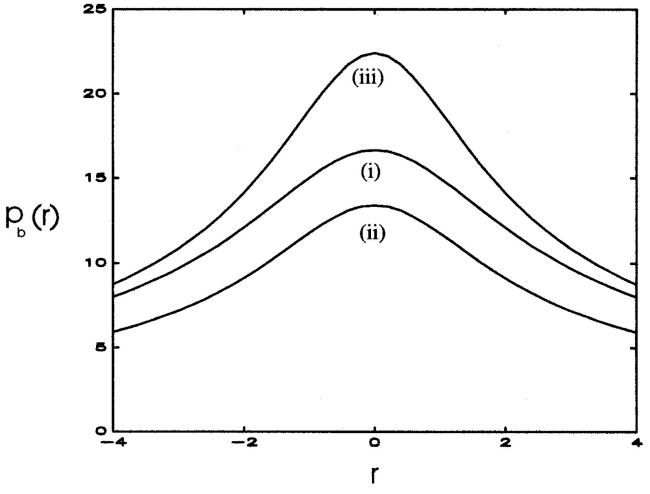

Fig. 9 The pressure $p_b(r)$ at the rigid boundary for a bubble with $\varepsilon = 100$ and $\delta = 0.0$ initiated at $\gamma = 2.0$ from the rigid wall. (i) At initiation of the bubble ($t = 0.0$), (ii) just prior to jet impact ($t = 2.164$), and (iii) just after jet impact ($t = 2.173$)

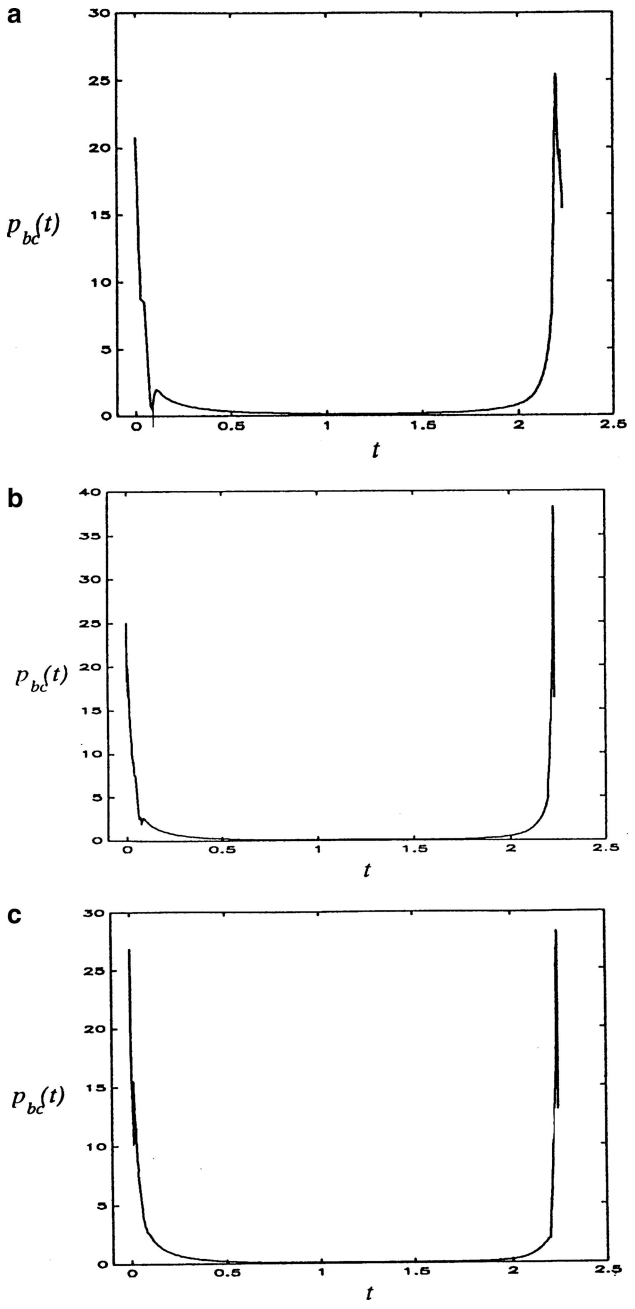

Fig. 10 The pressure $p_{\mathrm{bc}}(t)$ at the center point of the rigid boundary versus time t for the bubble with $\varepsilon = 100$ and $\delta = 0.0$ initiated at **a** $\gamma = 1.5$, **b** $\gamma = 1.3$, and **c** $\gamma = 1.2$, respectively

It is also pertinent to note that in real-life situations, a shock wave would be set up if the bubble initially expands at a speed larger than the sound speed of the surrounding liquid medium. This may happen for cases with large values of the strength parameter ε. The initial shock travels well ahead of the bubble surface. While the amplitude of the pressure pulse generated by the shock wave on the wall is usually much larger than that due to liquid jet impingement, its duration is much shorter and associated impulse smaller. This is a key reason to go for the simpler incompressible flow model, as we have done here and as done by others. The incompressible flow model is not able to account for the effects due to the initial shock wave. This should be borne in mind when interpreting the pressure results in all incompressible flow computations.

5 Summary

The jet impact transforms the originally singly-connected bubble to a toroidal one and yields a circulation to the flow around the toroidal bubble. A toroidal bubble modelling is presented by introducing a vortex ring seeded inside the bubble torus to account for the circulation of the flow. The velocity potential is then decomposed as the potential of the vortex ring and a remnant continuous potential. The remnant potential satisfies the Laplace equation and thus can be modelled by the boundary-integral method. The modelling obliviates the need for an explicit domain-cut and its associated numerical treatments, such as the intersecting and matching of the cut with the bubble surface. Consequently, a minor reconstruction of the bubble surface is needed at the jet impact zone to render the transformation to toroidal geometry compared to what may be required by Best [23] and Pearson et al. [25, 26] to accommodate the domain cut. In principle, we expect lower numerical error to be introduced by our procedure.

An important advantage of the present approach is that it can be extended with relative ease to three-dimensional cases as compared to the domain-cut approach. In the three-dimensional case, the velocity potential is decomposed into the potential of the vortex ring and a remnant potential, and the bubble surface and the remnant potential are updated using (17) and (18). The only major difference is that the vortex ring may be no longer circular, and its velocity has to be calculated numerically [36]. The results of Zhang et al. [36] agreed with that of this axisymmetric modelling. In this manuscript, good agreement is found with the results of Best and Blake et al. for circulation strength, timings of events, and bubble profiles. This further validates the present model, and the 3D implementation of Zhang et al. as well as the model of Best et al.

The algorithm is applied to study the collapse behavior of gas bubbles near a rigid boundary. Solutions are obtained for bubbles that are initiated as close as one Rayleigh maximum radius R_m from the rigid boundary. The following features of the evolution of toroidal bubbles are observed. The bubble continues to collapse (or show a reduction in volume) for a very short time after jet penetration. In this short period of time, the cross-sectional area of the impact region increases rapidly to the diameter of the liquid jet, whilst the rest of the bubble surface shrinks slowly. Upon reaching its minimum volume, the bubble begins to rebound (re-expand in volume). The bubble is attracted towards the wall during its rebounding.

The pressure history at the wall is calculated for a bubble initiated at various distances from the wall. The wall pressure is at first peak at the bubble inception, with near hydrostatic pressure over much of the expansion and collapse phases, and at a very sharp second pressure peak during the time of jet impact. The second peak is significantly larger than the first one for the bubble at its initial minimum volume. Therefore, the liquid jet has significant potential for causing damage to a surface. There also appears to be an optimal initiation distance for which the liquid jet thus formed is most damaging. The optimum stand off is found to be around $\gamma = 1.3$ in the absence of buoyancy.

Acknowledgements The authors want to express their sincere thanks to the referees of this paper and Professor J. R. Blake for their valuable suggestions.

References

1. Benjamin, T.B., Ellis, A.T.: The collapse of cavitation bubbles and pressure thereby produced against solid boundary. Philos. Trans. R. Soc. Lond. A. **260**, 221–240 (1966)
2. Guerri, L., Lucca, G., Prosperetti, A.: A numerical method for the dynamics of non-spherical cavitation bubbles, Proc. 2nd Int. Colloq. on Drops and Bubbles, p. 175. CA (1981)
3. Blake, J.R., Taib, B.B., Doherty, G.: Transient cavities near boundaries. Part 1. Rigid boundary. J. Fluid Mech. **170**, 479 (1986)
4. Baker, G.R., Moore, D.W.A.: The rise and distortion of a two-dimensional gas bubble in an inviscid liquid. Phys. of Fluids. **1**(9), 1451 (1989)
5. Best, J.P., Kucera, A.: A numerical investigation of non-spherical rebounding bubbles. J. Fluid Mech. **245**, 137 (1992)
6. Brujan, E.A., Keen, G.S., Vogel, A., Blake, J.R.: The final stage of the collapse of a cavitation bubble close to a rigid boundary. Phys. of Fluids. **14**(1), 85 (2002)
7. Blake, J.R., Gibson, D.C.: Growth and collapse of a vapour cavity near a free surface. J. Fluid Mech. **111**, 123 (1981)
8. Blake, J.R., Taib, B.B., Doherty, G.: Transient cavities near boundaries. Part 2. Free surface. J. Fluid Mech. **181**, 197 (1987)
9. Blake, J.R., Hooton, M.C., Robinson, P.B., Tong, P.R.: Collapsing cavities, toroidal bubbles and jet impact. Philos. Trans. R. Soc. Lond. A **355**, 537–550 (1997)
10. Wang, Q.X., Yeo, K.S., Khoo, B.C., Lam, K.Y.: Strong interaction between buoyancy bubble and free surface. Theoret. and Comput. Fluid Dynamics **8**, 73–88 (1996a)
11. Wang, Q.X., Yeo, K.S., Khoo, B.C., Lam, K.Y.: Nonlinear interaction between gas bubble and free surface. Computers & Fluids **25**, No. 7, 607 (1996b)

12. Chahine, G.L.: Numerical modeling of the dynamic behavior of bubble in nonuniform flow field. In: ASME Symp. on Numerical Methods for Multiphase Flows, Toronto (1990)
13. Chahine, G.L., Perdue, T.O.: Simulation of the three dimensional behaviour of an unsteady large bubble near a structure. In: Wang, T.G. (ed.) Drops and Bubbles, 3rd Int. Colloq., Monterey, CA, pp. 188–199. Amer. Inst. of Phys. (1988)
14. Wilkerson, S.A.: A boundary integral approach to three dimensional underwater explosion bubble dynamics. Ph.D. Dissertation, Johns Hopkins University, Baltimore, MD (1990)
15. Harris, P.J.: A numerical model for determining the motion of a bubble close to a fixed rigid structure in a fluid. Int. J. Numer. Methods Eng. **33**, 1813 (1992)
16. Harris, P.J.: A numerical method for predicting the motion of a bubble close to a moving rigid structure. Commun. Numer. Methods Eng. **9**, 81 (1993)
17. Wang, Q.X.: The numerical analyses of the evolution of a gas bubble near an inclined wall. Theoret. & Comput. Fluid Dynamics **12**, 29–51 (1998)
18. Wang, Q.X.: Numerical simulation of violent bubble motion. Phys. of Fluids **16**(5), 1610–1619 (2004)
19. Pozrikidis, C.: Numerical simulation of three-dimensional bubble oscillations by a generalized vortex method theoret. and comput. Fluid Dynamics **16**(2), 151–169 (2002)
20. Wang, C., Khoo, B.C.: An indirect boundary element method for three-dimensional explosion bubbles. J. Comput. Phys. **194** (2), 451–480 (2004)
21. Plesset, M.S., Prosperetti, A.: Bubble dynamics and cavitation. Annu. Rev. Fluid Mech. **9**, 145 (1977)
22. Blake, J.R., Gibson, D.C.: Cavitation bubbles near boundaries. Annu. Rev. Fluid Mech. **19**, 99–123 (1987)
23. Best, J.P.: The formulation of toroidal bubbles upon collapse of transient cavities. J. Fluid Mech. **251**, 79–107 (1993)
24. Best, J.P.: The rebound of toroidal bubbles. In: Blake, J.R., Boulton-Stone, J.M., Thomas, N.H. (eds.) Bubble Dynamics and Interface Phenomena, Fluid Mechanics and its Applications, vol. 23, pp. 405–412. Kluwer Academic Publishers, Dordrecht (1994)
25. Pearson, A., Cox, E., Blake, J.R., Otto, S.R.: Bubble interactions near a free surface. Eng. Anal. Bound. Elem. **28**(4), 295–313 (2004a)
26. Pearson, A., Blake, J.R., Otto, S.R.: Jets in bubbles. J Eng. Math. **48**(3–4), 391–412 (2004b)
27. Zhang, S., Duncan, J.H., Chahine, G.L.: The final stage of the collapse of a cavitation bubble near of a rigid wall. J. Fluid Mech. **257**, 147–181 (1993)
28. Zhang, S., Duncan, J.H.: On the non-spherical collapse and rebound of cavitation bubble. Physics of Fluids **6**(7), 2352–2362 (1994)
29. Szymczak, W.G., Roger, J.C.W., Solomon, J.M., Berger, A.E.: A numerical algorithm for hydrodynamic free boundary problems. J. Comput. Phys. **106**, 319–336 (1993)
30. Pedley, T.J.: The toroidal bubble. J. Fluid Mech. **32**, 97–112 (1968)
31. Lundgren, T.S., Mansour, N.N.: Vortex ring bubbles. J. Fluid Mech. **72**, 391–399 (1991)
32. Taib, B.B.: Boundary integral methods applied to cavitation bubble dynamics. Ph.D. Thesis, Univ. of Wollongong, NSW, Australia (1985)
33. Abramowitz, M., Stegun, I.A.: Handbook of Mathematical Functions. Dover, NY (1965)
34. Birkhoff, G., Zarantonello, E.H.: Jet, Cavities and Wakes. Academy Press, NY (1957)
35. Keller, J.B., Milewski P.A., Vanden-Broeck, J.M.: Breaking and merging of liquid sheets and filaments. J. Eng. Math. **42**(3–4), 283–290 (2002)
36. Zhang, Y.L., Yeo, K.S., Khoo, B.C., Wang, C.: 3D jet impact and toroidal bubbles. J. Comput. Phys. **166**, 336–360 (2001)